Supporting Information

Cobalt confined within nitrogen-doped porous carbon to enhance the redox kinetics and cycling stability of zinc-iodine batteries

Yongzhi Chen[a], Zhongyang Pan[a], Xiaobo Xu[b], Xinyang Wang[b], Feili Lai[a,*]

[a]*State Key Laboratory of Metal Matrix Composites*, *School of Materials Science and Engineering*, *Shanghai Jiao Tong University*, *Shanghai 200240, P. R. China*

[b] *Zhejiang Hanwei Technology Co., Ltd.*, *Hangzhou 311121, P. R. China*

* Corresponding authors (E-mail: feililai@sjtu.edu.cn)

Experimental Section

Synthesis of nitrogen-doped porous carbon (NPC) and nitrogen-doped porous carbon with cobalt cluster (NPC-Co)

Typically, 0.1 mmol of cobalt(II) chloride hexahydrate ($CoCl_2 \cdot 6H_2O$, 99.9%, Macklin) was dissolved in 60 mL of deionized water, followed by the addition of 4.5 g of zinc gluconate (98%, Macklin). The mixture was stirred for 10 min to form a homogeneous solution, then rapidly frozen using liquid nitrogen and freeze-dried for 24 h. The obtained solid precursor was transferred to a crucible and placed at the center of a tubular furnace. An open crucible containing 10 g of urea (99%, Macklin) was positioned upstream. The sample was pyrolyzed at 950 °C for 1 h under a nitrogen atmosphere with a heating rate of 5 °C min^{-1}. After cooling to room temperature, the as-pyrolyzed product was acid-washed in 0.5 M dilute hydrochloric acid (HCl, AR) for 1 h to remove excess cobalt and residual inorganic impurities, followed by thorough washing with deionized water until neutral pH was reached. The final product was collected after drying at 60 °C for 6 h and denoted as NPC-Co. NPC was prepared using the same procedure, except that $CoCl_2 \cdot 6H_2O$ was not added.

Preparations of NPC-Co@I_2 and NPC@I_2

The NPC-Co@I_2 composite was prepared via a melt-diffusion method. Typically, NPC-Co and elemental iodine were mixed at a mass ratio of 1:3 and sealed in a glass vial, then heated at 120 °C for 6 h. After cooling to room temperature, the mixture was further dried in an oven at 60 °C for 3 h to remove excess iodine. The NPC@I_2 composite was prepared using the same procedure.

Materials and structural characterizations

The crystal structures were analyzed using X-ray diffraction (XRD, MiniFlex 600) with Cu Kα radiation. The degree of graphitization in NPC and NPC-Co was examined using a confocal Raman spectrometer (Renishaw inVia Qontor). The iodine contents in NPC@I_2 and NPC-Co@I_2 were determined by thermogravimetric analysis (TGA, TA Instruments 550). Nitrogen adsorption-desorption isotherms were measured using a surface area and porosity analyzer (Micromeritics ASAP 2460), and the Brunauer-Emmett-Teller (BET) surface areas of NPC and NPC-Co were calculated accordingly. The morphologies and microstructures of NPC, NPC-Co, and NPC-Co@I_2 were observed using scanning electron microscopy (SEM, TESCAN Mira3). X-ray photoelectron spectroscopy (XPS, Thermo Scientific K-Alpha) was used to investigate the elemental compositions and chemical states of NPC@I_2 and NPC-Co@I_2.

Electrochemical measurements

A slurry was prepared by mixing sodium alginate (as an aqueous binder) and acetylene black with the active material at a mass ratio of 8:1:1, using deionized water as the solvent. The resulting slurry was coated onto titanium foil with an active material loading of 0.8-1.1 mg cm^{-2}. The electrodes were then dried at 60 °C for 6 h. CR2032-type coin cells were assembled in ambient air using zinc foil as the anode, a glass fiber membrane as the separator, and 80 μL of 2 M $ZnSO_4$ as the electrolyte. After assembly, the cells were allowed to rest for 12 h before electrochemical measurements. Galvanostatic charge/discharge tests were conducted using a LAND-CT2001A battery tester within a voltage window of 0.6-1.6 V (*vs.* Zn/Zn^{2+}). Cyclic voltammetry (CV) was performed on a CHI660E electrochemical workstation at scan rates ranging from

1 to 20 mV s^{-1} within the same voltage range. Electrochemical impedance spectroscopy (EIS) was also carried out on the CHI660E, over a frequency range of 0.01 Hz to 1 MHz. Specific capacities were calculated based on the mass of iodine.

Calculation of the b values and ratio of pseudo-capacitive contribution

The kinetic behavior was analyzed based on cyclic voltammetry (CV) measurements. The relationship between the peak current (i) and the scan rate (v) can be described by the following equation:

$$i = a\,v^{b} \tag{S1}$$

where a and b are adjustable parameters. By taking the logarithm of both sides of Eq. (S1), the equation can be rewritten as:

$$log\,(i) = log\,(a) + b\,log\,(v) \tag{S2}$$

The parameter b can be determined from the slope of the linear fitting of log(i) versus log(v), which provides insight into the charge-storage mechanism.

To further quantify the capacitive and diffusion-controlled contributions, the current response (i) at a given potential can be separated into two components according to:

$$i = k_1 v + k_2 v^{1/2} \tag{S3}$$

where $k_1 v$ represents the surface-controlled capacitive contribution, and $k_2 v^{1/2}$ corresponds to the diffusion-limited Faradaic process. By rearranging Eq. (S3), the equation can be expressed as:

$$i/v^{1/2} = k_1 v^{1/2} + k_2 \tag{S4}$$

Accordingly, the value of k_1 can be obtained from the slope of the linear fitting of $i/v^{1/2}$

versus $v^{1/2}$, enabling quantitative evaluation of the capacitive contribution.

Supplementary figures

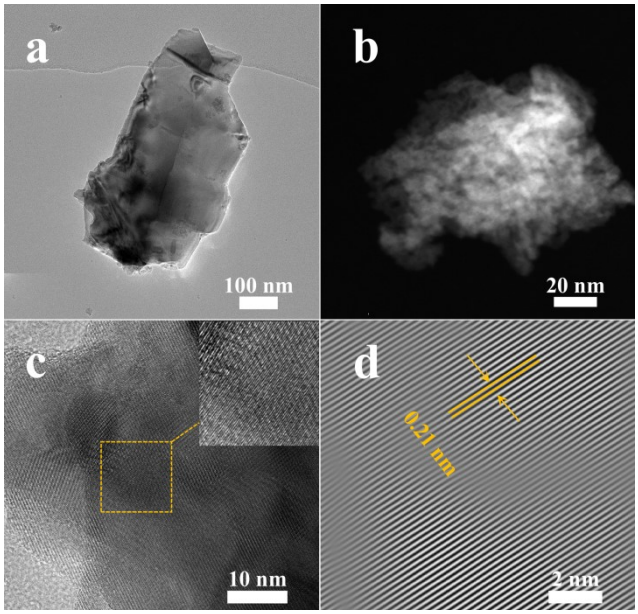

Fig. S1. Morphology and lattice features of NPC-Co. (a) TEM, (b) HAADF-STEM, (c) HRTEM, and (d) inverse FFT images of NPC-Co.

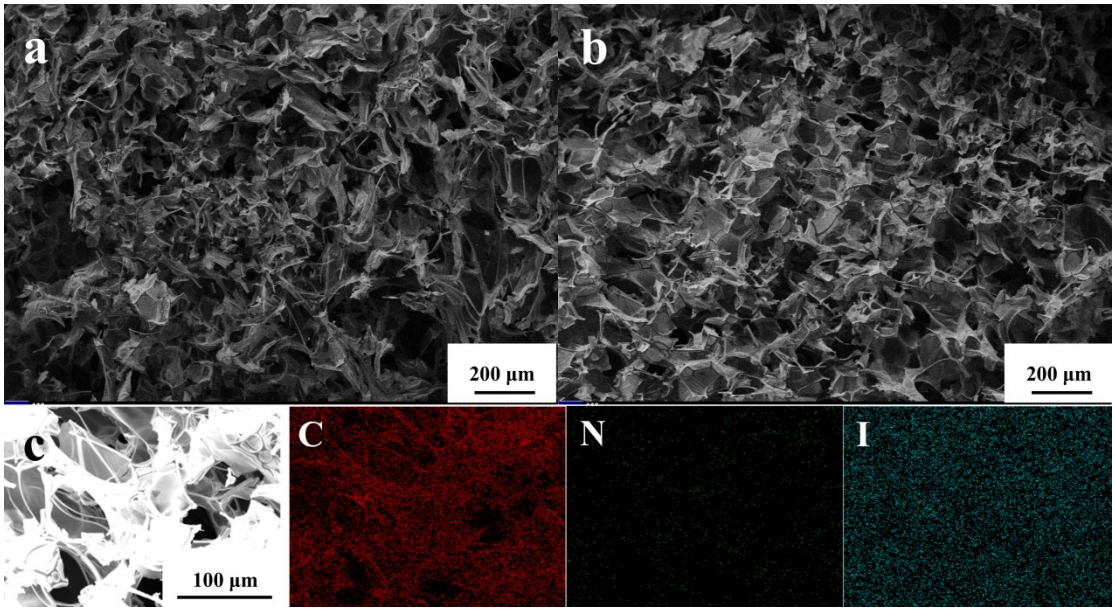

Fig. S2. Morphology of NPC and NPC@I_2. SEM images of (a) NPC and (b) NPC@I_2. (c) SEM image and corresponding EDS elemental mappings of NPC@I_2.

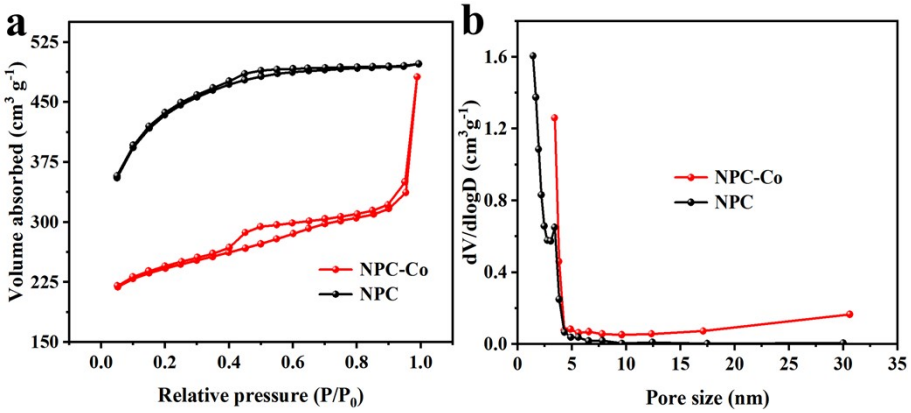

Fig. S3. Structural characterization of NPC and NPC-Co. (a) Nitrogen adsorption-desorption isotherms, and (b) pore size distributions of NPC and NPC-Co.

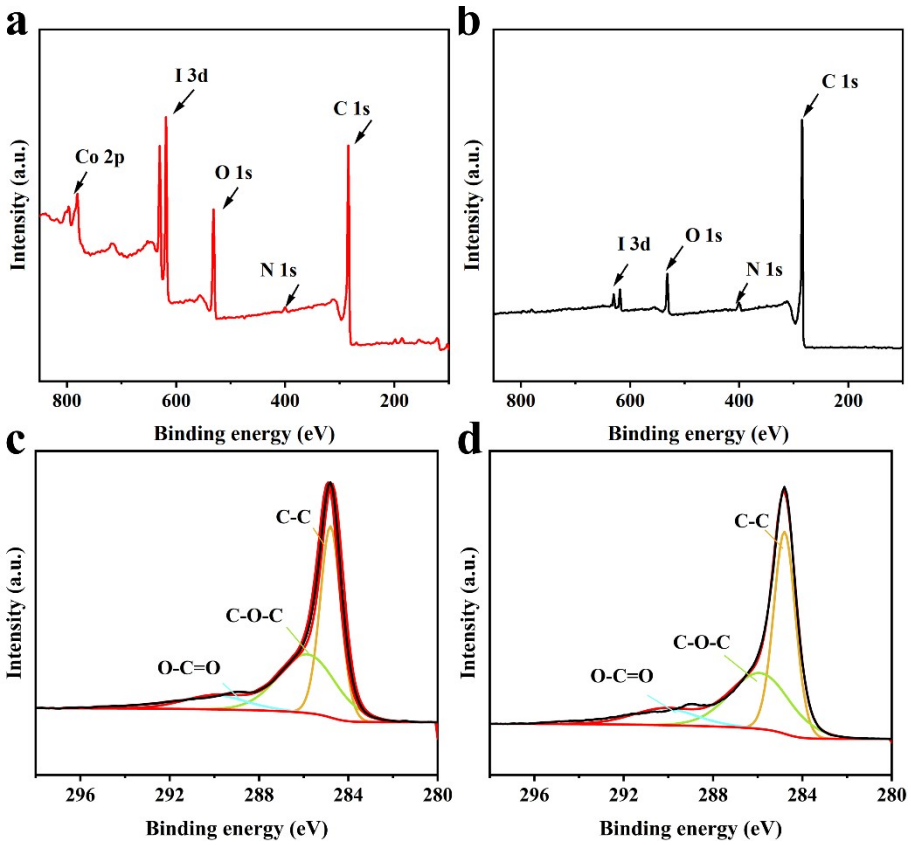

Fig. S4. XPS characterization of NPC-Co@I_2 and NPC@I_2. (a, b) Survey spectra of NPC-Co@I_2 and NPC@I_2. (c, d) High-resolution C 1s spectra of NPC-Co@I_2 and NPC@I_2.

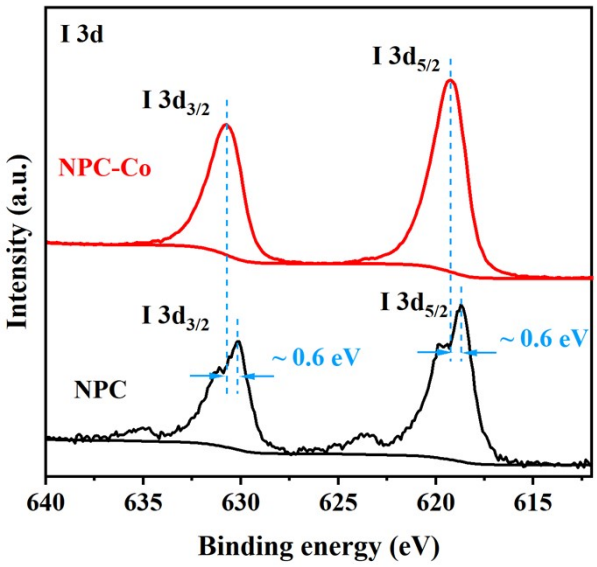

Fig. S5. Iodine chemical-state analysis of NPC-Co@I_2 and NPC@I_2. High-resolution I 3d XPS spectra of NPC-Co@I_2 and NPC@I_2.

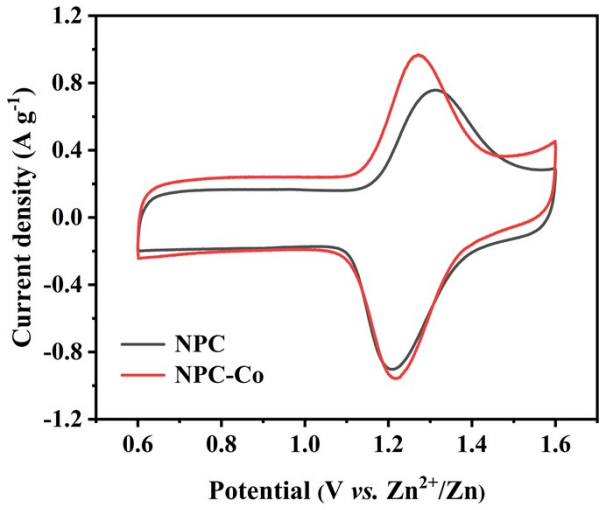

Fig. S6. Normalized CV curves of Zn//NPC-Co@I_2 cells and Zn//NPC@I_2 cells at 1 mV s^{-1}.

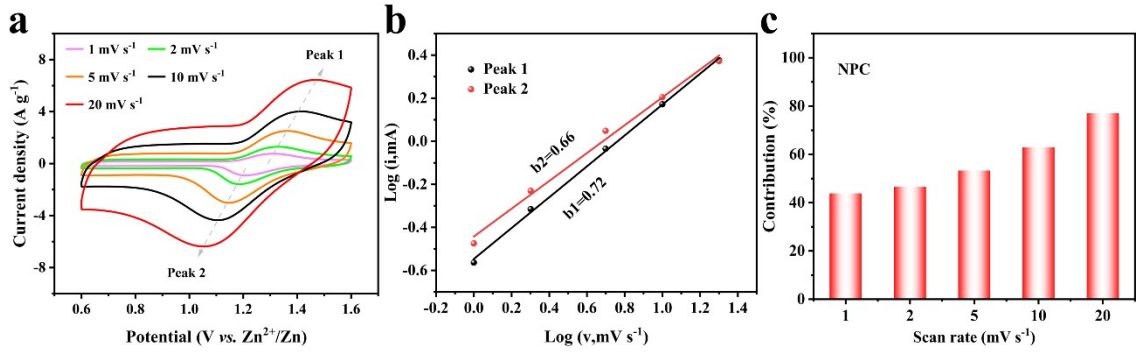

Fig. S7. Kinetic analysis of the Zn//NPC@I_2 battery. (a) CV curves of the Zn//NPC@I_2 battery at various scan rates. (b) Calculated b-values for the redox peaks of the Zn//NPC@I_2 battery. (c) Estimated capacitive contribution ratios at different scan rates.

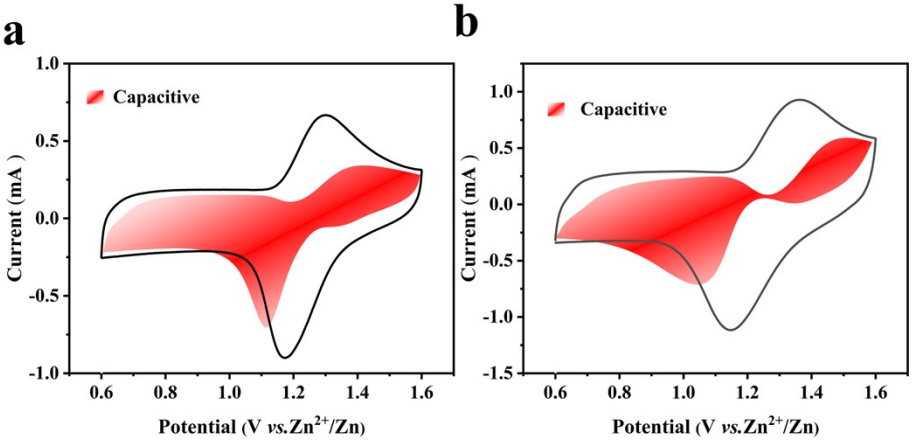

Fig.S8. Capacitive-controlled CV curves of (a) NPC-Co and (b) NPC at 5 mV s^{-1}.

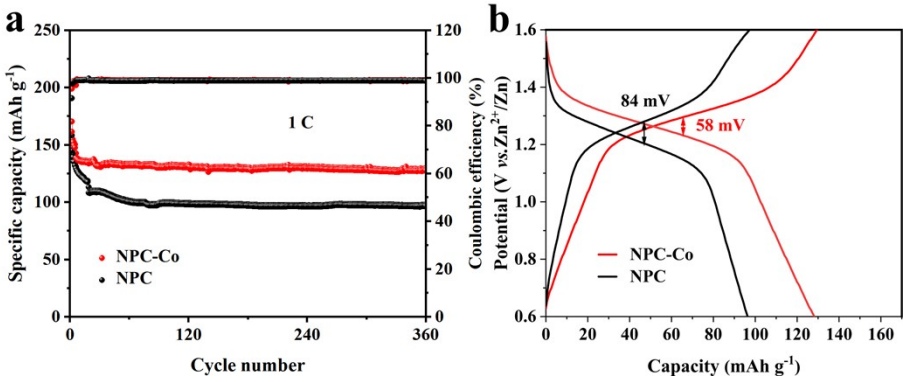

Fig. S9. Cycling performance of the Zn//NPC@I_2 battery. (a) Long-term cycling performance at 1 C. (b) Galvanostatic charge-discharge profiles at the 200th cycle.

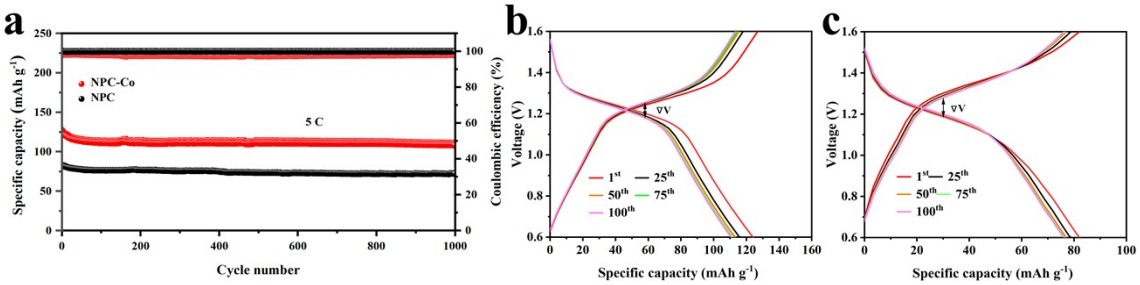

Fig. S10. Cycling performance of Zn//NPC-Co@I_2 and Zn//NPC@I_2 batteries. (a)

Long-term cycling performance at 5 C. (b) Galvanostatic charge discharge curves of Zn//NPC-Co@I_2 and (c) NPC@I_2 cathode at different cycles.

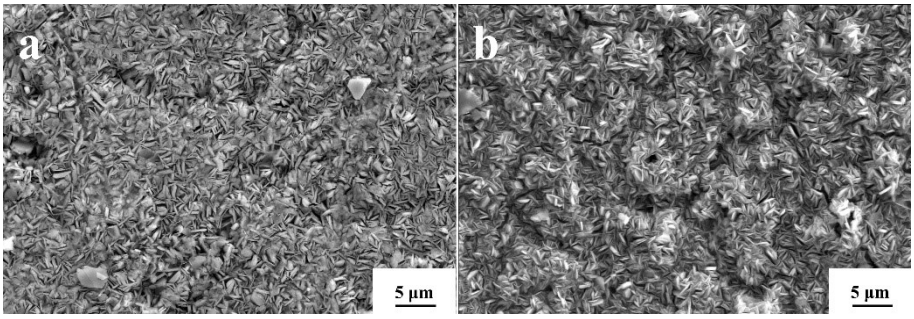

Fig. S11. SEM images of Zn anodes after 100 cycles at 1 C for Zn anodes from (a) Zn//NPC-Co@I_2 cells and (b) Zn//NPC@I_2 cells.

Table S1. Comparison of representative iodine cathodes reported for aqueous Zn–I_2 batteries and this work.

Ref.	Host	Rate	Capacity (mAh g^{-1})	Cycling performance

1	I_2–NPC-900	10 C	177.7	80.9% retention after 10,000 cycles
2	HOPG/I_2	5 A g^{-1}	278	97.6% retention after 15,000 cycles
3	Functionalized graphene	5 A g^{-1}	150	96.7% retention after 2000 cycles
4	FeCoNi@I_2	3 A g^{-1}	94.7	94.7 mAh g^{-1} after 14,000 cycles
5	PPC–CH/I_2	2 A g^{-1}	99.9	>88% retention after 9000 cycles
6	I_2@NHPC	5.0 C	166.7	85.2% retention after 10,000 cycles
Ref.	**Host**	**Rate**	**Capacity (mAh g^{-1})**	**Cycling performance**
7	I_2@GP-CMTs	12 A g^{-1}	101	86.8% retention after 1000 cycles

8	I_2@C-50	5 A g^{-1}	116.7	66% retention after 10,000 cycles
9	NS-YP80F@I_2	5 C	125	125 mAh g^{-1} after 800 cycles
10	NMC/I_2	0.1 A g^{-1}	91	80.7% retention after 100 cycles
11	I_2-AC-6	5 A g^{-1}	89.7	90% retention after 6000 cycles
12	N-LPC/I_2	0.1 A g^{-1}	127	127 mAh g^{-1} after 100 cycles
This work	NPC-Co@I_2	5 C	109.3	97.6 mAh g^{-1} after 1500 cycles

Note: For this work, 1 C = 211 mA g^{-1}.

References

1 D. Yu, A. Kumar, T. A. Nguyen, M. T. Nazir and G. Yasin, *ACS Sustain. Chem. Eng.*, 2020, **8**, 13769.

2 J. Zhang, Q. Dou, C. Yang, L. Zang and X. Yan, *J. Mater. Chem. A*, 2023, **11**, 3632.

3 H. X. Dang, A. J. Sellathurai and D. P. J. Barz, *Energy Storage Mater.*, 2023, **55**, 680.

4 Y. Gao, Y. Liu, X. Guo, J. Zhang, C. Zhou, F. Li, Z. Xu, Z. Zhao, Z. Xing, P. Rao, Z. Kang, X. Tian and X. Shi, *Adv. Funct. Mater.*, 2024, **35**, 2421714.

5 C. Chen, C. Liu, H. Huang, S. Luo, M. Xie, D. Ma, F. Zeng and X. Liang, *Electrochim. Acta*, 2026, **559**, 148584.

6 Z. Gong, C. Song, C. Bai, X. Zhao, Z. Luo, G. Qi, X. Liu, C. Wang, Y. Duan and Z. Yuan, *Sci. China Mater.*, 2023, **66**, 556.

7 S. Chai, J. Yao, Y. Wang, J. Zhu and J. Jiang, *Chem. Eng. J.*, 2022, **439**, 135676.

8 W. Li, K. Wang and K. Jiang, *J. Mater. Chem. A*, 2020, **8**, 3785.

9 W. Feng, Y. Wang, F. Tian, Z. Liu, X. Wei, C. Ma, G. Ma, Z. Li, D. Kong and L. Zhi, *Energy Storage Mater.*, 2024, **73**, 103812.

10 M. Zhang, Y. Hou, Y. Zhu, M. Ren, X. Cai, Q. Liu, C. Qiao, W. Liu and J. Yao, *J. Electroanal. Chem.*, 2025, **976**, 118798.

11 Y. Zhang, X. Zhang, X. Li, C. Chen, D. Yu and G. Zhao, *J. Alloys Compd.*, 2024, **976**, 173041.

12 Y. Ji, J. Xu, Z. Wang, M. Ren, Y. Wu, W. Liu, J. Yao, C. Zhang and H. Zhao, *J. Electroanal. Chem.*, 2023, **931**, 117188.